CIRP Journal of Manufacturing Science and Technology 41 (2023) 490–500

Contents lists available at ScienceDirect

CIRP Journal of Manufacturing Science and Technology

journal homepage: www.elsevier.com/locate/cirpj

Multiresponse optimization of performance indicators through Taguchi-grey relational analysis in EDM of cemented carbide

Ahmet Tolunay Işık [a], Ramazan Çakıroğlu [b,*], Mustafa Günay [a]

[a] Department of Mechanical Engineering, Faculty of Engineering, Karabük University, Karabük, Turkey
[b] Department of Design, Vocational School of Technical Sciences, Gazi University, Ankara, Turkey

ARTICLE INFO

Available online xxxx

Keywords:
EDM
Cemented carbide
Keyway
Grey relational analysis
Optimization

ABSTRACT

Cemented carbide is mostly used in the mold and tool industry due to their high hardness, temperature and wear resistance, and it is very difficult to shape with conventional machining methods. Because, during the machining of certain geometry from these materials, microcracks on surface and flaking at the machined edges due to their brittleness as well as rapid tool wear mostly due to their high hardness occur. In this case, EDM is considered one of the most suitable machining technologies for brittle material such as carbides, as it provides a non-contact shaping with electrical sparks between the tool and the workpiece. This study focused on the simultaneous optimization of the most important performance indicators namely material removal rate, tool wear rate and surface roughness in creating a keyway on WC-15Co material with the die-sinking EDM. As a result of experiments using copper electrode, the impacts on performance indicators of discharge current, pulse time and pulse interval were investigated with 3D surface topography images. It was determined that the peaks and craters formed on the machined surface expanded with the increase of pulse time, and the decreased with the increase in the pulse interval. As a result of the Taguchi-grey relational analysis (TGRA) application, discharge current of 6 A, pulse time of 25 µs and pulse interval of 100 µs were found as optimum parameters. ANOVA results showed that Ip, Ton and Toff affected GRG values by 44.23%, 28.77% and 5.87%, respectively. A 23.95% improvement in performance indicators was achieved thanks to the TGRA multiresponse optimization.

© 2023 CIRP.

Introduction

There are two fundamental groups of ceramics as traditional and advanced ceramics. First, traditional ceramics, consisting of an inorganic, non-metallic solid containing clay, silica and feldspar, is a group of low-functional materials used in daily work (glass, concrete, clay) and not preferred for different applications. Second, advanced ceramics include oxides, carbides, nitrides, silicide, borides, etc., also called high-performance ceramics, high-tech ceramics, engineering ceramics and fine ceramics [1]. These materials differ from traditional ceramics in their higher strength, adaptable properties, improved toughness, higher operating temperatures, and these properties offer the production of modern ceramic components [2]. Ceramic components can be generally manufactured in four different stages: material preparation, machining, sintering and finishing. Although ceramic parts are produced close to the final shape by various molding and heat treatment methods, conventional machining operations such as lapping, grinding, turning, milling, drilling may be required. Thus, machining is used to bring ceramic parts to the desired shape, finish surface, strength and size. However, difficulties such as shortened tool life, long finish time, excessive residual material, crack formation in most conventional machining accounts for approximately 60–80% of the production cost of ceramic parts [3,4].

Among advanced ceramics, ceramic matrix carbides have growing potential as cutting tools and mold parts in environments where high mechanical strength, wear resistance and melting point are required. Machining these material with unconventional machining methods compared to conventional machining methods is a way to minimize tool wear, material waste, and crack formation [5–7]. Therefore, advanced manufacturing methods are required to create complex shapes, functional parts and proportional micro-holes in ceramic materials for the production of industrial equipment [8]. The need to process ceramic materials has led to the development of advanced production methods and thus the production of advanced ceramic products, which are highly needed in the domestic and foreign market, has been facilitated and the production process has accelerated [9]. Advanced

* Corresponding author.
E-mail address: rcakiroglu@gazi.edu.tr (R. Çakıroğlu).

https://doi.org/10.1016/j.cirpj.2023.01.012
1755-5817/© 2023 CIRP.

manufacturing methods such as electrical discharge machining (EDM), laser machining (LBM) and ultrasonic machining (USM) can perform metal removal using various forms of energy without cutting tools and/or abrasive particles. Considering its advantages such as ability to process in complex shapes obtaining of the desired dimensional precision and fine surface quality among all alternatives, the EDM method is an extremely suitable technology for the machining of electro-conductive materials [10]. EDM is manufacturing technology that is characterized as non-contact and thermal machining. That is, sparks that occur in pulsed high-frequency current between the tool (electrode) and the workpiece cause the material to melt and evaporate with the thermoelectric effect, and thus the chip removal process occurs. Moreover, this technology is one of the most suitable solutions for low cost and high accuracy machining of materials that are difficult to machine and brittle [11].

It is understood from the literature that various ceramic materials are processed using EDM processes such as classical EDM, powder mixed EDM, wire EDM and μEDM. These studies have shown that the effects of machining parameters such as discharge current (Ip), pulse duration (Ton), pulse interval (Toff) and reference voltage on performance criteria such as metal removal rate (MRR), tool wear rate (TWR) and surface roughness are mostly investigated [8,12]. For instance, in EDM of WC with copper tool, low Ip and Ton are recommended for low Ra, while high discharge current and low reference voltage and pulse duration are suggested for low TWR, but the need for simultaneous parameter optimization is emphasized [13]. In recent years, studies on the optimization of processing parameters in EDM of various materials have reported that increased discharge current and pulse time increase TWR and Ra and improve MRR [14,15]. Lin et al. investigated the variation of MRR, TWR and surface roughness by changing the discharge current (1–9 A) and the pulse time (3–500 μs) in the EDM of WC with Cu tool. In experiments using negative polarity, it was stated that MRR increased as the pulse time decreased and the discharge current increased. It was also emphasized that the discharge energy required for the material removal mechanism (melting/evaporation) at low Ip was not sufficient due to the high melting temperature of the WC (3000 °C) [16]. Lee and Li examined the effects of discharge current (16–64 A) and pulse time (1.6–2.5 μs) on surface morphology and surface integrity in EDM of tungsten carbide with Cu-WC electrode. It has been observed that increasing high temperature gradients as the Ip value increases, causes the formation of microcracks due to high thermal stresses and a looser microstructure up to a depth of 15 μm. In addition, the increase in the discharge energy caused deeper craters, spherical projections and high roughness on the surface [17]. In an interesting study, the effects of discharge current, pulse time, and pulse interval on the main machinability indicators were considered at the machining of tool steel using the EDM turning. As a result of multiple optimization using Taguchi-grey relational analysis, it was stated that Ip= 3 A, Ton= 8 μs, Toff= 6 μs are the most suitable machining parameters [18]. Agarwal et al. focused on EDM of AISI D2 tool steel at different levels of discharge current (4–70 A), pulse time (100–300 μs), duty cycle (80–90%) and reference voltage (40–60 V). As a result of Jaya optimization algorithm, the highest MRR was found to be 33.3650 mm3/min at 10 A, 100 μs, duty cycle of 90%, 40 V levels, while 6.7840 A, 300 μs, duty cycle of 90%, 40 V values were suggested for the lowest TWR [19]. Amorim et al. investigated the impacts on MRR, TWR and Ra of discharge current, pulse time, duty cycle and open circuit voltage in EDM by copper-tungsten electrode of WC-Co material. They have prepared usable parameter-result guides for carbide material by optimizing the parameters in three steps [20]. Singh and Sharma evaluated the powder-mixed EDM of tungsten carbide comparatively using GRA, grey-fuzzy and grey-adaptive neuro fuzzy inference (grey-ANFIS) optimization systems. In the experiments, the effects of discharge current, pulse time, dielectric level and dielectric pressure on MRR, TWR, aerosol (smoke) density and dielectric consumption were investigated. From the validation experiments and estimation results, the optimization with the lowest error level was determined as grey-ANFIS (5.76%), GRA (12.19%) and grey-fuzzy (15.41%) respectively. It was stated that the parameters 6 A, 50 μs, 40 mm, 0.6 kg/cm^2 were the most suitable machining parameters in all of the multiple optimizations [21]. Sarıkaya and Yılmaz examined the effects on machinability indicators (MRR, TWR, taper and overcut) of the discharge current (6–24 A), dielectric pressure (20–80 bar) and tool rotation speed (100–400 rpm) parameters in the micro-EDM of AISI 304 stainless steel. The authors stated that 10.18 A, 58.7879 bar and 100 rpm values are the best conditions for micro drilling as a result of multiple optimization with RSM [22].

After the literature review, it has been seen that there is no comprehensive study on the creation of a distinctive geometry with EDM on a cemented carbide material, which is one of the materials that are difficult to machine. In this study, the effects of the most important EDM parameters (Ip, Ton and Toff) on the performance criteria (tool wear rate, metal removal rate and surface topography) in the opening of a keyway in accordance with DIN 6885 standard onto WC-Co material were investigated experimentally and statistically. In addition, it is aimed to optimize the machining parameters for minimum TWR and surface roughness and maximum MRR in the shaping of cemented carbide material with EDM. In this context, the selected performance criteria were optimized simultaneously using the Taguchi-based grey relational analysis technique. The results obtained will facilitate the selection of parameters in the industrial processing of ceramic materials with EDM, and will contribute significantly to filling the gap in the above-mentioned literature.

Research details and analysis

Experimental procedure

Experimental studies were carried out with Furkan brand “K1 Z-NC EDM” electro-erosion machine found in Gazi University laboratory. Cemented carbide (WC-15Co) with a diameter of 16 mm was used as the workpiece material. Mechanical properties of cemented carbide; hardness, density, particle size, fracture strength are 1400 Hv(30), 13.95 g/cm3, 0.8 μm and 4000 MPa, respectively. In line with the research purpose, tools (electrode) made of electrolytic copper material were prepared in order to reach the dimensions of the Form A type keyway (5×5x20 mm), which were selected in accordance with the DIN6885 standard. The workpiece material is fixed with the help of a vise attached to the electro-erosion machine and the electrode is fixed with a specially made tool holder. The images of workpiece material, tool, machine used in experimental studies and EDM process are shown in Fig. 1.

The odorless and high flash point (102 °C) fluid used as a dielectric in the experiments has a density of 0.760 kg/m^3 and a kinematic viscosity of 1.910 mm^2/s. The dielectric fluid was continuously sent to the processing zone with a pressure of 35 kPa using the lateral washing method. The machining depth, i.e. the keyway depth, is set at 3 mm. Tool retraction distance has been adjusted as 4.5 mm in order to clean the debris in the processing zone more easily during operation. The tool polarity is positive and the workpiece polarity is negative, and the open circuit voltage is 130 V and the reference voltage (gap) is 60 V in the die-sinking electro-erosion machine.

Discharge current (Ip), pulse time (Ton) and pulse interval (Toff), which are the most effective processing parameters in EDM operations, were determined as variables. As a result of the preliminary experiments and literature review, three different levels were selected for these variables. Taguchi L27 experimental design was applied according to the determined variable levels and the performance indicators were analyzed by repeating the experiments. In Fig. 2, the varying machining parameters and the parameters held constant are given in a schematic representation of the electrical discharge machining.

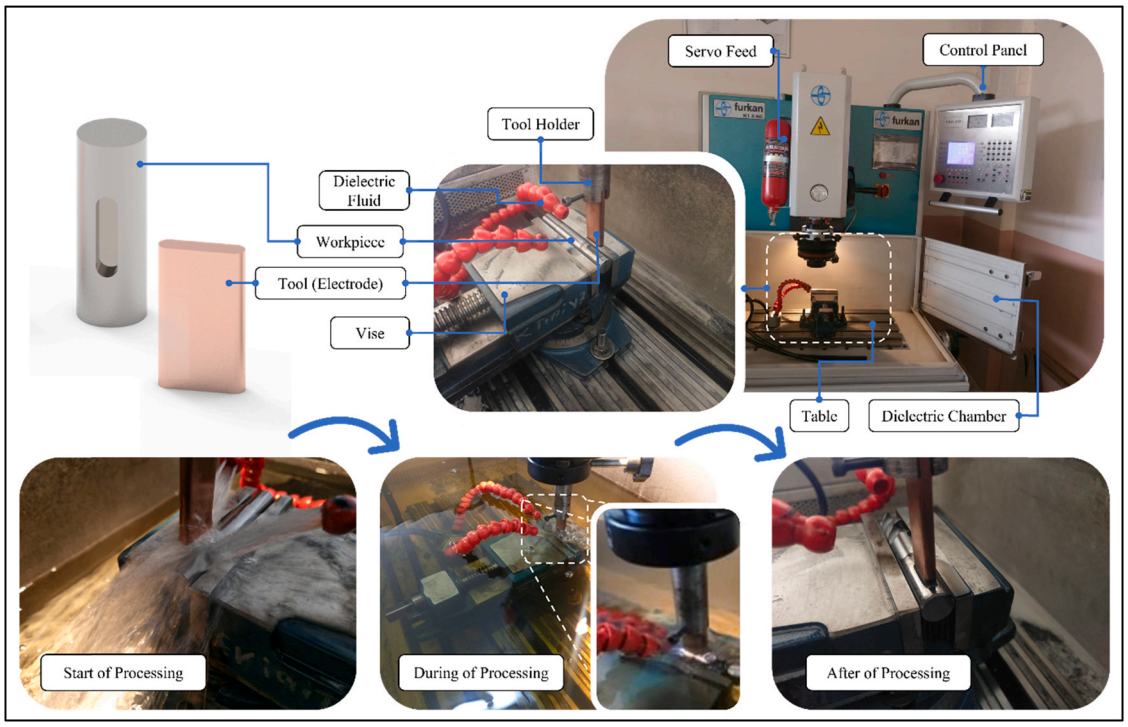

Fig. 1. Experimental equipment.

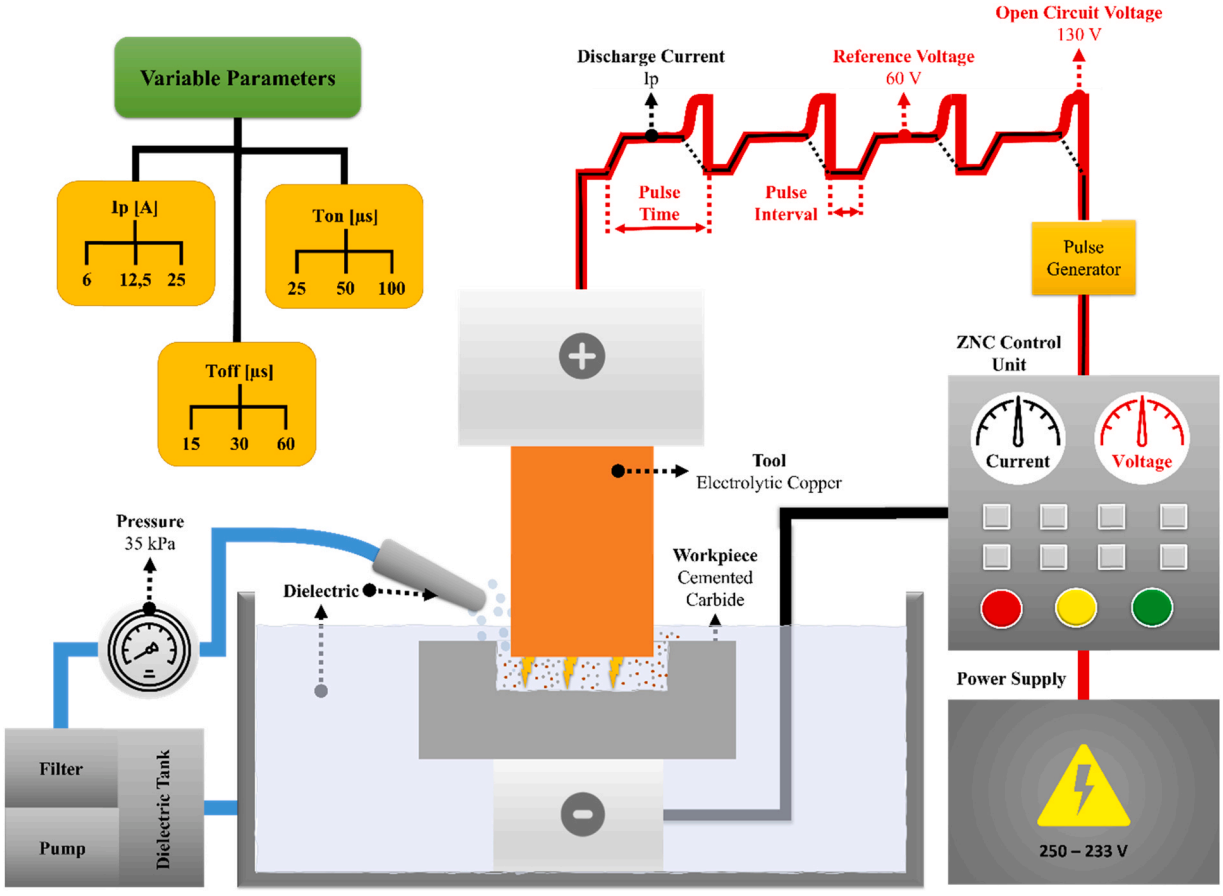

Fig. 2. Display of processing conditions.

Table 1
Normalization approaches.

The biggest is better, (Eq. (3)):	The smallest is better, (Eq. (4)):	The nominal is better, (Eq. (5)):
$x_{ij} = \frac{y_{ij} - \min(y_{ij})}{\max(y_{ij}) - \min(y_{ij})}$	$x_{ij} = \frac{maks(y_{ij}) - y_{ij}}{\max(y_{ij}) - \min(y_{ij})}$	$x_{ij} = 1 - \frac{y_{ij} - y_j^*}{\max(y_{ij}) - \min(y_{ij})}$

Measurement of performance indicators

In all experiments, mass losses were calculated by measuring workpiece and tool (electrode) weights with a digital balance with 0.001 g sensitivity before and after the experiment. Machining time data were obtained with the help of the counter integrated in the machine. In line with these data, performance indicators namely MRR (in g/min) and TWR (in g/min) were calculated by using Eqs. (1) and (2), respectively.

The average surface roughness (Ra) was taken as the roughness criterion in the evaluation of the surface quality obtained in the processing of WC-Co material by die-sinking EDM. MarSurf M300 mobile measurement device was used for roughness measurements. During the measurements, the cutting length was chosen as 0.8 mm and the sampling length as 5.6 mm. After each experiment, three measurements were made at the base of the keyway and the Ra results were analyzed by taking the arithmetic average. In addition, 3D surface images were taken at the measurement range of 2500 × 2000 µm from the processing area in order to topographically evaluate the surface quality.

$$\mathrm{MRR} = \frac{w_b - w_a}{t} \tag{1}$$

$$\mathrm{TWR} = \frac{w_{tb} - w_{ta}}{t} \tag{2}$$

In Eqs. (1) and (2), w_b and w_a are the weights of the workpiece in grams before and after machining, w_{tb} and w_{ta} are the weights of the tool electrode in grams before and after the machining, and t is the machining time in minutes [23].

Analysis and multiresponse optimization

As a result of the experimental studies, various statistical techniques were used to analyze the effects of current, pulse time and pulse interval parameters on MRR, TWR and Ra. In order to determine the effect levels of the variables on the performance indicators, variance analysis was performed at the 95% confidence interval. Since micro cracks and craters of different sizes are possible surface deformations in the parts processed with EDM, the surface integrity of the ceramic workpiece was examined with 3D topographic measurements. Finally, optimum processing parameters were found by applying Taguchi-grey relational analysis (TGRA) methodology. The optimization process is explained in detail below.

As the measurement methods of the performance indicators (MRR, TWR and surface roughness) taken into account in the EDM process are different, the measurement units are also different. Therefore, it is necessary to bring the results with different units into a comparable series. In this point, Taguchi method uses unusual experimental designs, namely orthogonal arrays, to review the responses by a minimal number of experiments and allows regulatory of independent variable for improving the responses. But, this technique cannot be used to obtain best process parameters for multiple responses, it only helps to find optimal conditions for a single response [24,25]. Hence, it is crucial to optimize all responses simultaneously for maximum efficiency in machining processes where every response is critically important. Within this scope, special techniques such as response surface method [26], genetic algorithm [27], particle swarm optimization [28], grey relational analysis (GRA) [29] can be used. However, Taguchi-based GRA technique is the most commonly used multiple response optimization in practice, as it is easy to implement as well as competent and flexible [30]. In TGRA methodology, the first step in the optimization of the processing parameters for the determined performance indicators or responses is normalization. The aim here is to reduce the experimentally measured outcome data to a value range of 0–1 and to keep all data on an equal and evaluable scale. For this, three different approaches are applied and the equations given in Eqs. (3)–(5) are used according to the expected situation from performance indicators (Table 1) [31,32].

In Eqs. (3)–(5), x_{ij} is the normalized result data, $\min(y_{ij})$ is the smallest value in the data range, $\max(y_{ij})$ is the largest value in the data range, y_j^* is the target value, and y_{ij} is defined as y_i selected from j result data. As the next step of the analysis, if $x_0 = 1$ is defined as the reference sequence, the grey relational coefficients (GRC) are calculated with Eq. (6) in order to determine the closeness of x_{ij} to x_{0j}.

$$\gamma(x_{0j}, x_{ij}) = \frac{\Delta_{\min} + \zeta\Delta_{\max}}{\Delta_{ij} + \zeta\Delta_{\max}} \tag{6}$$

$\gamma(x_{0j}, x_{ij})$, grey relational coefficient between x_{ij} and x_{0j} in Eq. (6), $\Delta_{ij} = |x_{0j} - x_{ij}|$, $\Delta_{\min}$: smallest value in Δ_{ij}, $\Delta_{\max}$: largest value in Δ_{ij}, ζ coefficient is defined as [0,1] value range. As the GRC value increases, the closeness of $x_{ij}$to the reference value decreases. The ζ value is used to expand or compress the GRC range. As this value changes, the value of $\gamma(x_{0j}, x_{ij})$ will always change. However, since the effect of the ζ value on the grey relational analysis is very small, the order of the priority values of the result data will remain the same. For this reason, the ζ coefficient is usually taken as 0.5 [33].

In the analysis, the grey relational grade (GRG) is found with Eq. (7) in order to evaluate and predict the test results as a whole. GRG shows the best performance result to be achieved. Therefore, the highest GRG value gives the best performance result among the calculated criteria.

$$\Gamma(X_0, X_i) = \sum_{j=1}^{n} w_j \gamma(x_{0j}, x_{ij}) \tag{7}$$

$$\sum_{j=1}^{n} w_j = 1 \tag{8}$$

Γ in Eq. (7) is defined as the GRG value between X_0 and X_i, the grey relational coefficient $\gamma(x_{0j}, x_{ij})$ and the weight of the result factor w_j. If all outcome factors (n) are not of equal importance, GRG is calculated so that the total is w_j= 1 [34].

In the last step, the S/N ratio is calculated for grey relational grades using the Taguchi method. The S/N ratio shows the optimum levels of the input parameters. In this case, it is necessary to adopt the “the bigger is better” approach, as the highest GRG will give the best performance value. The S/N values for this approach are obtained using Eq. (9).

$$S/N = -10\log\left(\frac{1}{n}\sum_{i=1}^{n}\frac{1}{y_i^2}\right) \tag{9}$$

Here, y_i is the ith test result, n is the number of experiments [35,36]. A validation experiment is performed for the parameters obtained as a result of the optimization. Comparing the outcome data from the validation experiment with the original/initial

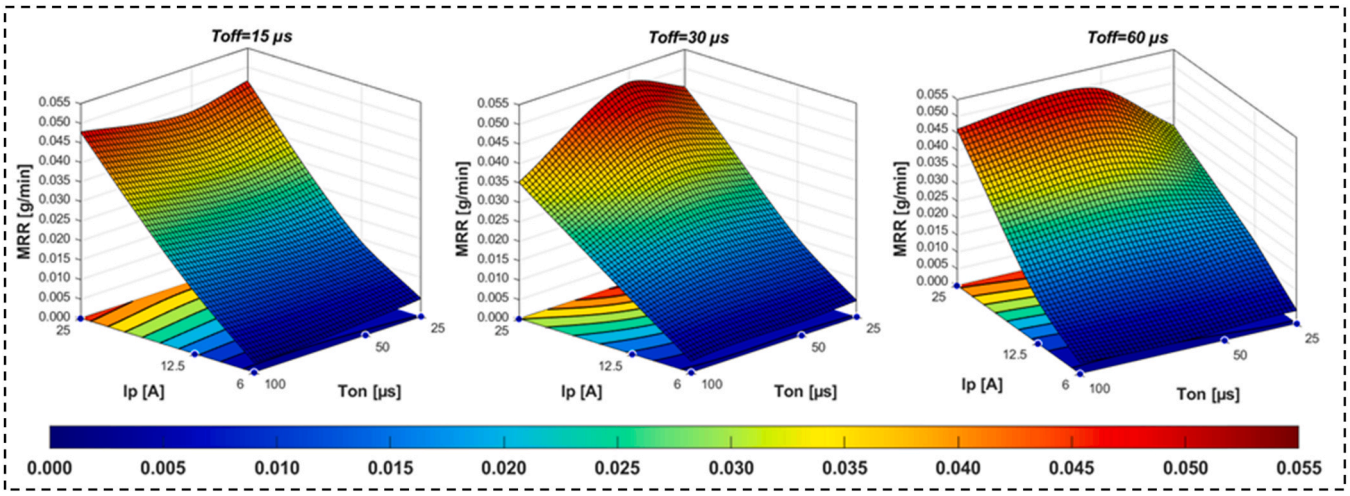

Fig. 3. Variation of MRR according to processing parameters; a) Toff = 15 µs, b) Toff = 30 µs, c) Toff = 60 µs.

experiment data presents the degree of reliability of the grey relational analysis.

Findings and discussion

Analysis of performance indicators

Roughness, tool life and machining speed are the most important criteria for the surface quality and machining cost of the parts produced with EDM technology. Therefore, improving MRR and TWR are factors that reduce production costs, and improving Ra are factors that increase surface quality. In this study, a keyway in DIN 6885 standard was cut on cemented carbide material using the classical EDM method. As a result of EDM experiments, the effects of discharge current, pulse time and pulse interval on the performance indicators were examined with the help of graphics. The graphics were created using the interpolation method with the help of Matlab R2021 program.

When the graphs in Fig. 3 are examined, it is clearly seen that the discharge current is the most effective variable on MRR. The increased discharge current causes an increase in the discharge energy, resulting in higher erosion with severe sparks. The melting and evaporation of the material during discharge and the expansion and shrinkage behaviors of the debris cloud is formed in the processing cavity because instantaneously changing forces (repulsive force). With this force, the debris is transferred from the processing zone to the dielectric medium [37]. Thus, the increase in discharge current increases the MRR at a greater rate than the increase caused by other parameters. While the highest MRR value was obtained as 0.05130 g/min at Ip= 25 A, Ton= 50 µs and Toff= 30 µs (Fig. 3b), the lowest MRR was calculated as 0.00256 g/min at Ip= 6 A, Ton= 100 µs and Toff= 15 µs. Despite the increase in the total discharge energy at high pulse time, the expansion in the plasma channel reduces the energy density in the processing cavity and reduces the heat energy per unit area in the processing zone [38]. Therefore, MRR decreased when the pulse time was long. When the pulse time is too short, MRR remains low because sufficient discharge energy cannot be provided.

On the other hand, MRR changes are compared in terms of pulse interval at peak discharge current (25 A). For the pulse interval of 30 µs (Fig. 3b), the magnitude order in MRR is obtained at 100 µs, 25 µs, and 50 µs, respectively. It is known that the increased pulse time increases the MRR by having the discharge energy that will rapidly melting and evaporate the material [39]. However, carbon accumulation on the electrode surface with increasing discharge energy slows down the spark mechanism [40], and therefore, the thick layered debris that remains on the processed surface before the evaporation and cannot be cleaned due to insufficient heat energy. Thus, a decrease occurred in MRR as a result of this formation which is generally occur at interaction the high pulse time-low pulse interval, similarly to the literature [41]. In pulse interval of 60 µs (Fig. 3c), the increase trend MRR values are 25 µs, 100 µs and 50 µs pulse times, respectively. Similarly, the increase of MRR as the pulse interval increases can be attributed to easier cleaning of debris and thick layer with the higher pulse interval. Meanwhile, the trend in MRR at the highest pulse time (100 µs) is in line with the increase in pulse interval. This result points to the importance of quickly clearing chips in the machining environment.

The change of TWR by processing parameters is shown with graphs in Fig. 4. When the graphs are examined, it can be seen that the discharge current is the most effective variable on TWR. Similar to the change in MRR, it is thought that the heat energy and repulsive force released by the increase in the discharge energy with increasing current also erodes the tool (electrode). In addition, it has been emphasized that the carbon separated from the dielectric liquid with the increasing pulse time reduces the wear by forming a protective layer on the electrode, when the tool is the anode [16]. In this case, it is clearly seen that TWR decreases as the pulse time increases (Fig. 4).

The highest TWR was calculated as 0.026548 g/min at Ip= 25 A, Ton= 25 µs and Toff= 15 µs level, while the lowest TWR was calculated as 0.000268 g/min at Ip= 6 A, Ton= 100 µs and Toff= 15 µs levels (Fig. 4a). When these graphs are examined, it is seen that TWR increases as the current increases and decreases as the pulse time increases. At 6 A and 12.5 A discharge currents, it is seen that the pulse interval does not cause sudden changes on the TWR. On the other hand, the heat released by the discharge energy may decrease rapidly in the high pulse interval, causing a carbon layer to form on the electrode. Besides, in case of the local heat generated by the low pulse time is very high, the pulse interval affecting the formation and solidification of the carbon layer may not be long enough [42]. As can be seen from the graphs, this phenomenon manifests itself as a decrease in TWR with an increase in the pulse interval.

Surface roughness (Ra) is the most critical performance criterion that determines the surface quality of the parts manufactured by machining. Fig. 5 shows the effects of pulse interval, pulse time and discharge current on Ra. The increase in discharge current causes deeper craters by transferring intense energy to the workpiece surface during machining, while the increase in pulse time causes larger craters due to the expansion in the plasma channel [18]. Thus, as can be seen from the graphs, Ra increased at a certain rate as the

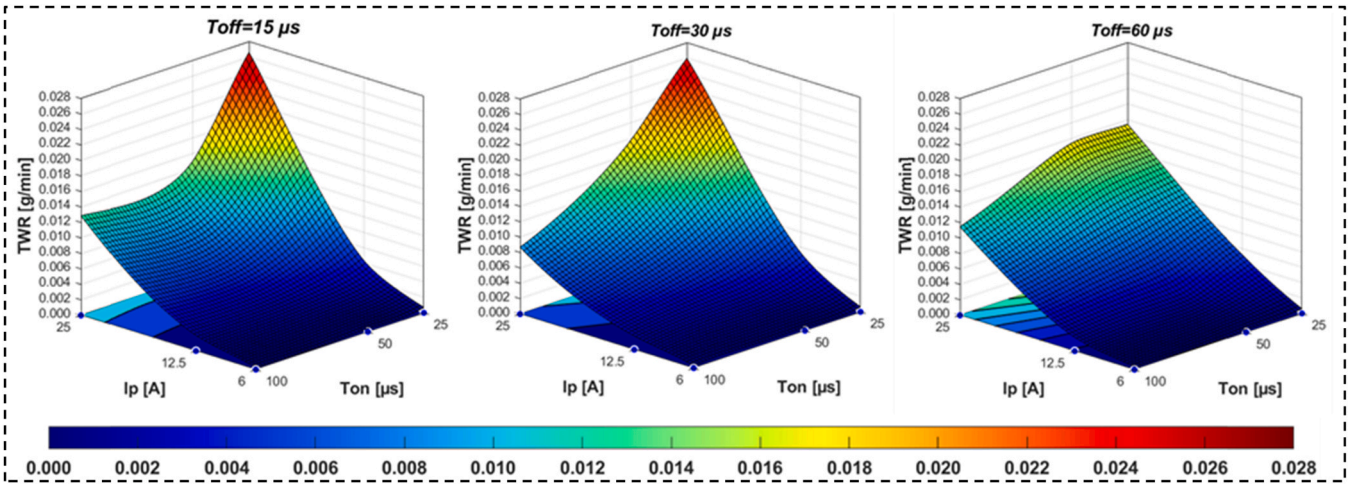

Fig. 4. Variation of TWR according to processing parameters; a) Toff = 15 µs, b) Toff = 30 µs, c) Toff = 60 µs.

discharge current and pulse time increased. On the other hand, Ra decreases as the pulse interval increases. Because the adhesion of debris on the tool or on the machined surface is minimized, resulting in a stable chip removal. However, Ra first increased and then decreased with increasing discharge current at 100 µs pulse time (Fig. 5b). This result was attributed to the short-circuit sparks generated during processing, which could not be removed, forming a thick layer in the processing zone [43]. Thus, the crater formation on the machined surface was formed in a complex form, causing an increase in roughness. The lowest Ra value was measured as 2291 µm at Ip= 6 A, Ton= 25 µs, Toff= 60 µs (Fig. 5c), while the highest Ra value was obtained as 8324 µm at Ip= 25 A, Ton= 100 µs and Toff= 15 µs (Fig. 5a).

In EDM, chips are removed from the material by melting and evaporation that occurs thanks to the sparks that occur in the closest position to the tool. This process can result in the formation of peaks and craters in random geometries that make up the surface morphology of the workpiece [44]. In this context, 3D surface topography of the machined parts was taken for the highest and lowest values of Ip, Ton and Toff parameters in order to examine the changes in surface morphology (Figs. 6 and 7). As can be seen from these figures, the amount of peaks (in red color) and craters (in green color) formed decreases and their size increases as the discharge current increases. This is because the energy transferred by the increased discharge current causes more melting and evaporation from the processing zone [45]. Decreased discharge current slows evaporation, that is, because sufficient heat cannot be produced, the molten material solidifies, causing the peak density to increase, as seen from Fig. 7. When Figs. 6a-b and 7a-b are examined, it is clearly seen that craters and peaks decrease when the pulse interval (Toff) is kept constant and the pulse time (Ton) is increased. Besides, the amount of energy dissipated per unit area decreases due to the increasing discharge diameter in parallel with the increase in the pulse time [46]. This prevents the formation of deep craters at high pulse time and increases the width of craters and peaks. On the other hand, increasing the pulse interval results in better debris removal and improves surface roughness.

Electro discharge machining is an ideal method for machining sensitive and complex parts. However, the recast layer, microcracks, craters and surface damage caused by high thermal energy occur in the processing region, which is considered as the disadvantage of this technique [47]. Figs. 8 and 9 shows examples from scanning electron microscope (SEM) micrographs of cut surface sections of the workpiece sample. The deposit formed after the discharge creates recast layer in the craters due to the high density of the WC-15Co (Fig. 9b). Although the diameters of the craters decrease depending on the depth, crack formation can

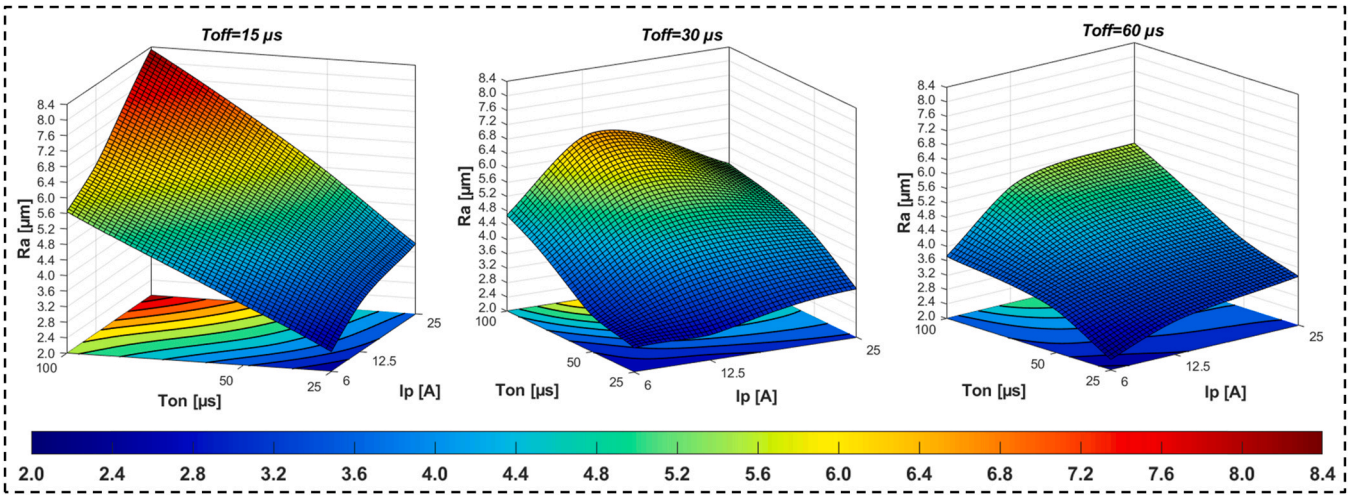

Fig. 5. Variation of Ra according to processing parameters; a) Toff = 15 µs, b) Toff = 30 µs, c) Toff = 60 µs.

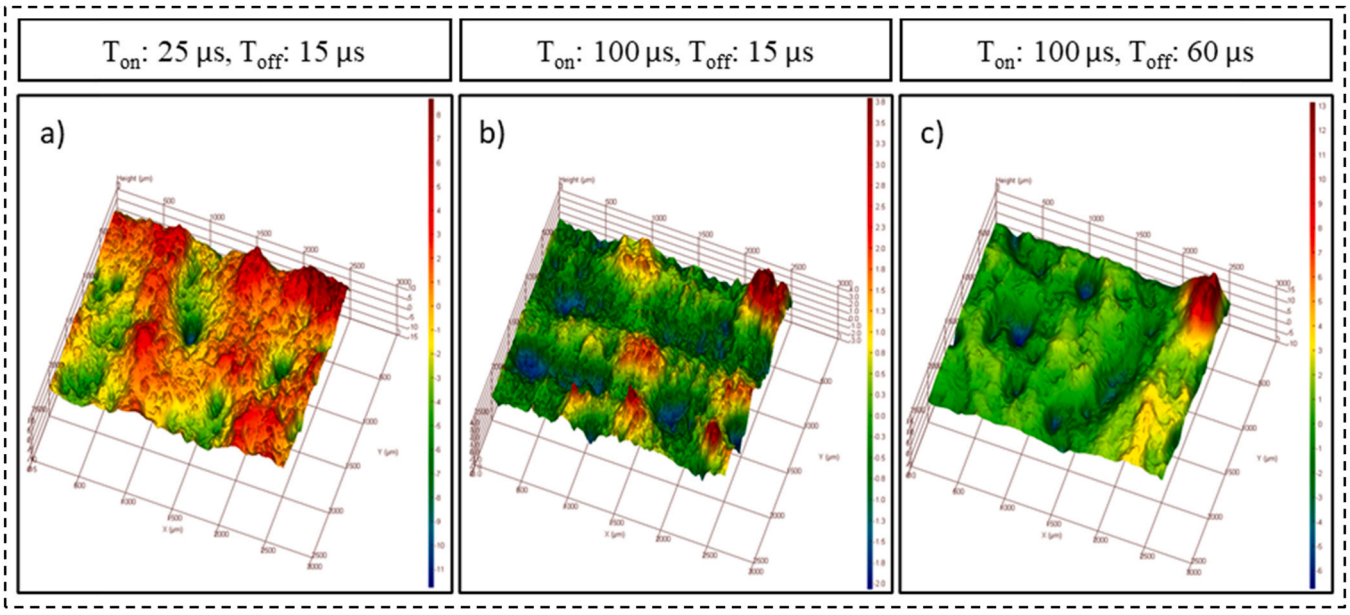

Fig. 6. Topography graphics of the processed samples (Ip = 6 A).

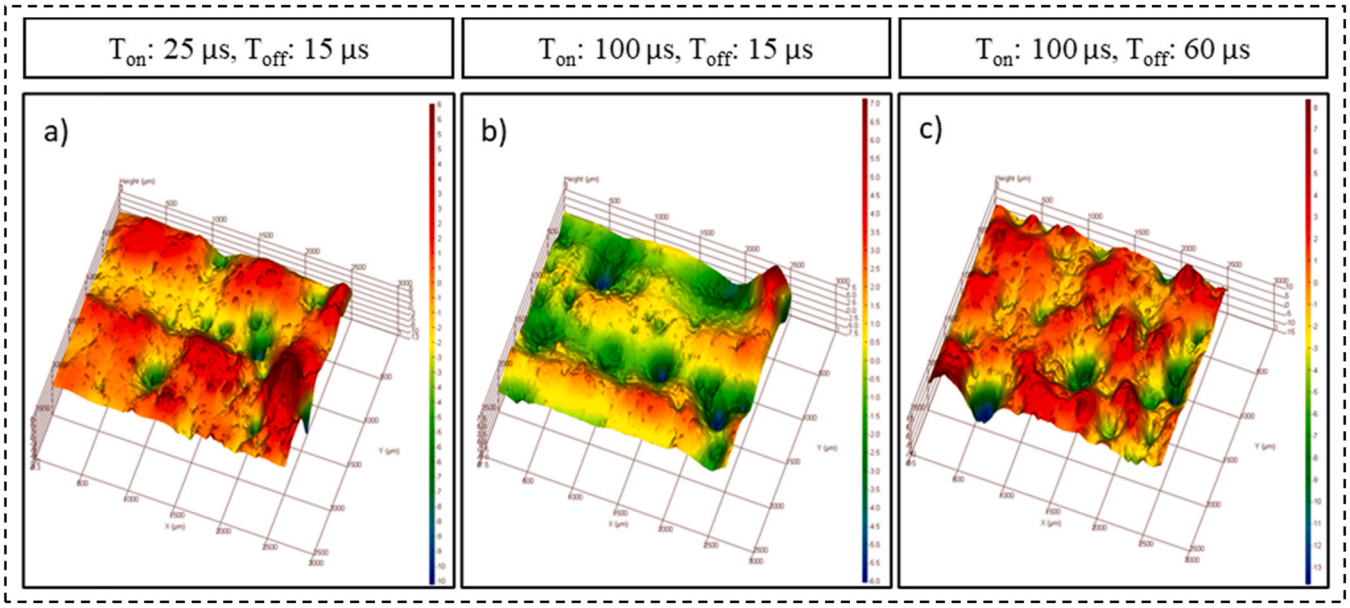

Fig. 7. Topography graphics of the processed samples (Ip = 25 A).

be observed with high thermal changes in craters that have formed a recast layer [48,49]. From Fig. 8a and b, the increase in crater width depending on the pulse on time is clearly visible. Therefore, the area of the crater regions surrounded by cracks was determined and shown in the percentage histogram plot in the figure. The average area of the craters increased (4213 µm^2 - 8963 µm^2) by 2.13 times as the pulse on time increased from 25 µs to 100 µs, namely when increasing four times. This trend in craters also caused an increase in surface roughness. Fig. 8c and d show the spattered EDM surface layer (SL), globules and micro-valleys, which are formed as a result of the inability to remove debris from the machining surface with the decrease in Toff value. Similarly, these formations also caused irregularity in the crater form and worsened the surface roughness. In conclusion, it can be said that the decrease in Toff contributes negatively to the surface quality, as can be seen from Fig. 5. At the same time, these formations on the crater surfaces caused a decrease in MRR and an increase in TWR. These results once again showed how important the multiple optimization technique is in the EDM of cemented carbide material.

The discharge current is seen as the most important process parameter affecting the thickness of the recast layer [50,51]. The thickness of the recast layer and the heat affected zone in EDM is usually very thin [52]. For example, in Fig. 9, the recast layer thickness is less than 33 µm. The hard recast layer, which is rare in the cross-sectional area given in Fig. 9b, increases the average layer thickness due to the high discharge current. It is seen that the microcrack and crater formed in the machining parameters determined in Fig. 9a and b do not penetrate the main part layer. In this case, the thermal stresses did not allow the formation of cracks that would affect the strength of the material.

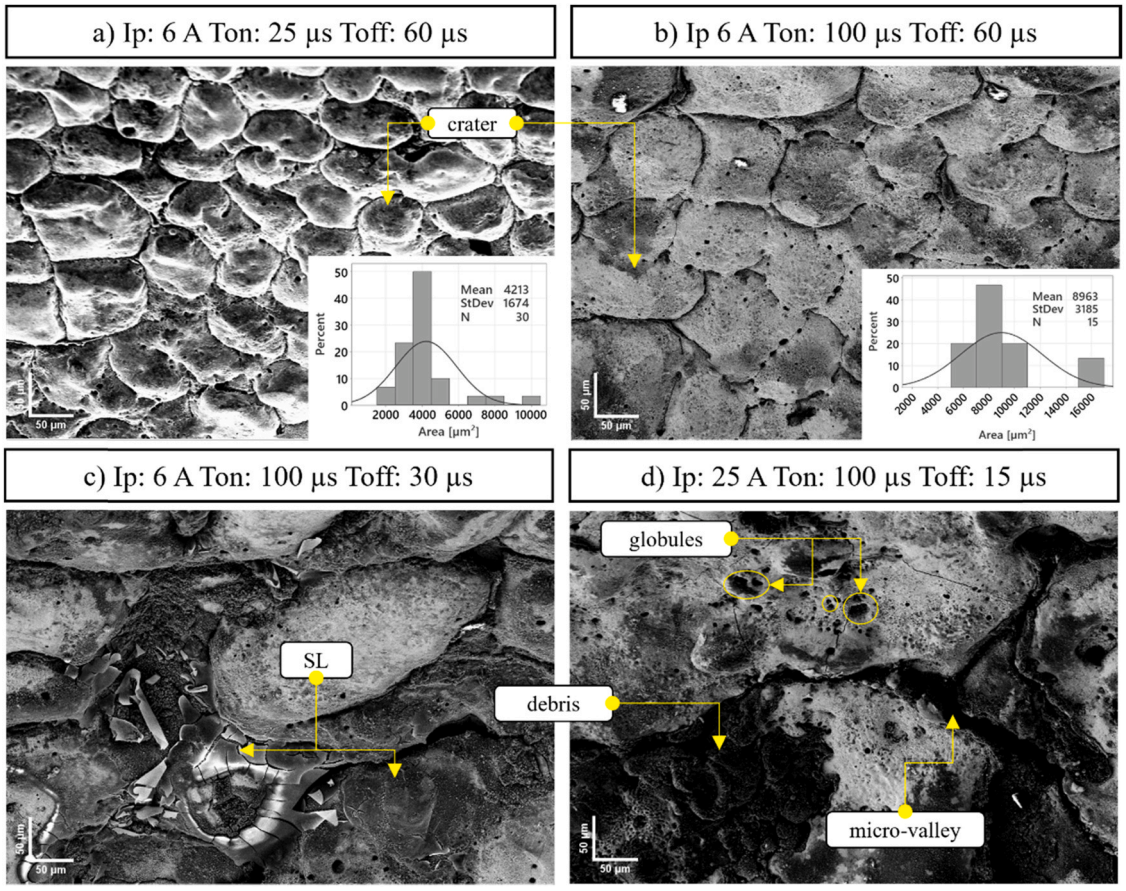

Fig. 8. SEM images of the machined surface.

TGRA results

By evaluating the experimental data, it was determined that the discharge current, pulse time and pulse interval have at different levels effects on the performance indicators (MRR, Ra, TWR) in die-sinking EDM of cemented carbide. On the other hand, since the units of these outputs are not the same, some difficulties arise in determining the optimum parameters. In order to easily overcome these difficulties, multiple optimization was made by applying Taguchi-based grey relational analysis. As explained in the previous section, the normalization approach was first determined for the performance indicator (response) in optimization. In this context, Eq. (3) is used to maximize MRR, Eq. (4) was used to minimize TWR and Ra. Grey relational coefficients were calculated using Eq. (6) by helps of the normalized MRR, TWR and Ra. Eq. (7) was used to calculate the grey relational degrees, which is the next step. In this study, since each outcome factor has equal importance (n = 3), w_j= 1/3 for each factor. Normalization, GRC, GRG and rank are given as GRA data for the performance indicators obtained in Table 2.

For the GRG values obtained, the S/N ratios calculated using Taguchi's "larger is better" approach (Table 3) and the main effect graphs in Fig. 10 were obtained. In this table, the highest value of the input parameters indicates the optimum level, while the delta column and the order of influence indicate the importance of the

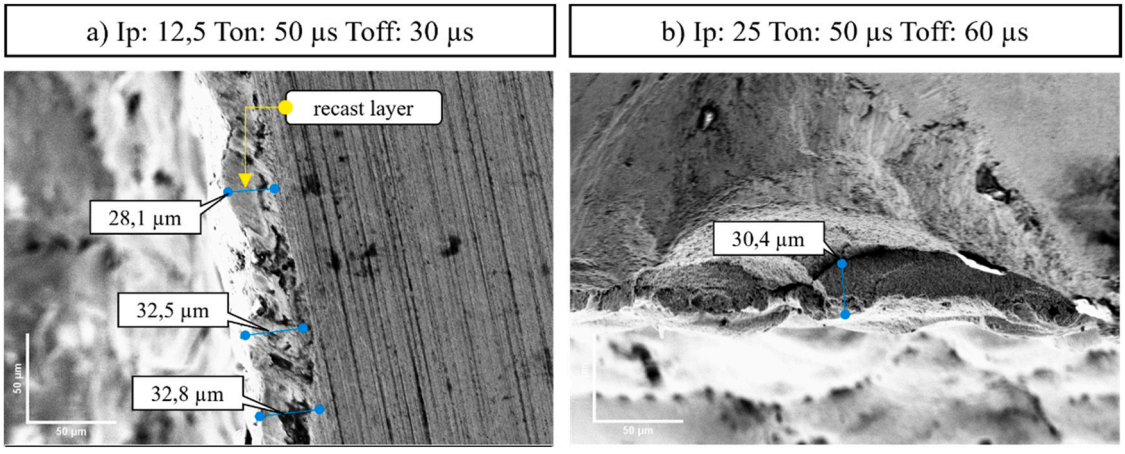

Fig. 9. SEM images of the machined surface section.

Table 2
Grey relational analysis results.

Exp. no	Exp. Results			Normalization			Grey Relational Coefficient			GRG	Rank
	MRR	TWR	Ra	MRR	TWR	Ra	MRR	TWR	Ra		
1.	0.00456	0.00069	2.508	0.041	0.984	0.964	0.343	0.969	0.933	0.748	2
2.	0.00419	0.00064	2.672	0.034	0.986	0.937	0.341	0.972	0.888	0.734	3
3.	0.00388	0.0006	2.291	0.027	0.987	1.000	0.339	0.975	1.000	0.772	1
4.	0.00349	0.00041	3.559	0.019	0.995	0.790	0.338	0.989	0.704	0.677	6
5.	0.00358	0.00041	3.022	0.021	0.994	0.879	0.338	0.989	0.805	0.711	4
6.	0.00318	0.00036	3.186	0.013	0.996	0.852	0.336	0.993	0.771	0.700	5
7.	0.00256	0.00027	5.644	0.000	1.000	0.444	0.333	1.000	0.474	0.602	20
8.	0.00296	0.00033	4.674	0.008	0.998	0.605	0.335	0.995	0.559	0.630	14
9.	0.00329	0.00035	3.724	0.015	0.997	0.762	0.337	0.993	0.678	0.669	9
10.	0.01428	0.00431	3.246	0.241	0.846	0.842	0.397	0.765	0.760	0.640	13
11.	0.0154	0.0052	2.707	0.263	0.812	0.931	0.404	0.727	0.879	0.670	8
12.	0.01534	0.00518	2.925	0.262	0.813	0.895	0.404	0.728	0.826	0.653	11
13.	0.01395	0.00251	4.456	0.234	0.915	0.641	0.395	0.854	0.582	0.610	19
14.	0.0165	0.00307	4.069	0.286	0.893	0.705	0.412	0.824	0.629	0.622	16
15.	0.01408	0.00249	3.545	0.236	0.916	0.792	0.396	0.855	0.706	0.653	12
16.	0.01586	0.00204	6.319	0.273	0.932	0.332	0.407	0.881	0.428	0.572	25
17.	0.01383	0.00182	6.527	0.231	0.941	0.298	0.394	0.894	0.416	0.568	27
18.	0.01275	0.00178	5.218	0.209	0.943	0.515	0.387	0.897	0.508	0.597	21
19.	0.04655	0.02655	3.806	0.903	0.000	0.749	0.837	0.333	0.666	0.612	18
20.	0.04534	0.02591	3.344	0.878	0.024	0.825	0.804	0.339	0.741	0.628	15
21.	0.03246	0.01738	3.351	0.613	0.349	0.824	0.564	0.434	0.740	0.579	22
22.	0.04342	0.015	5.485	0.838	0.439	0.471	0.756	0.471	0.486	0.571	26
23.	0.0513	0.0178	4.284	1.000	0.333	0.670	1.000	0.428	0.602	0.677	7
24.	0.04823	0.0174	3.877	0.937	0.348	0.737	0.888	0.434	0.655	0.659	10
25.	0.04778	0.01287	8.324	0.928	0.520	0.000	0.874	0.510	0.333	0.573	24
26.	0.03519	0.0087	5.144	0.669	0.679	0.527	0.602	0.609	0.514	0.575	23
27.	0.04613	0.01145	5.604	0.894	0.574	0.451	0.825	0.540	0.477	0.614	17

Table 3
GRG means for processing parameters.

Parameter	level1	level2	level3	Delta	Rank
Ip	0.6936*	0.6206	0.6097	0.0839	1
Ton	0.6706*	0.6533	0.6000	0.0706	2
Toff	0.6229	0.6460	0.6551*	0.0322	3
Total mean value of GRG=0.6413					

parameters. Accordingly, the *Ip1Ton1Toff3* test sequence indicates the optimum levels of the parameters (6 A discharge current, 25 µs pulse time and 60 µs pulse interval). With the help of the graphs in Fig. 10, the accuracy of the initial parameters was checked and the estimated GRG results were obtained. Estimated results for the specified EDM parameters are MRR= 0.003581 gr/min, TWR= 0.000414 gr/min and Ra= 2.291 µm.

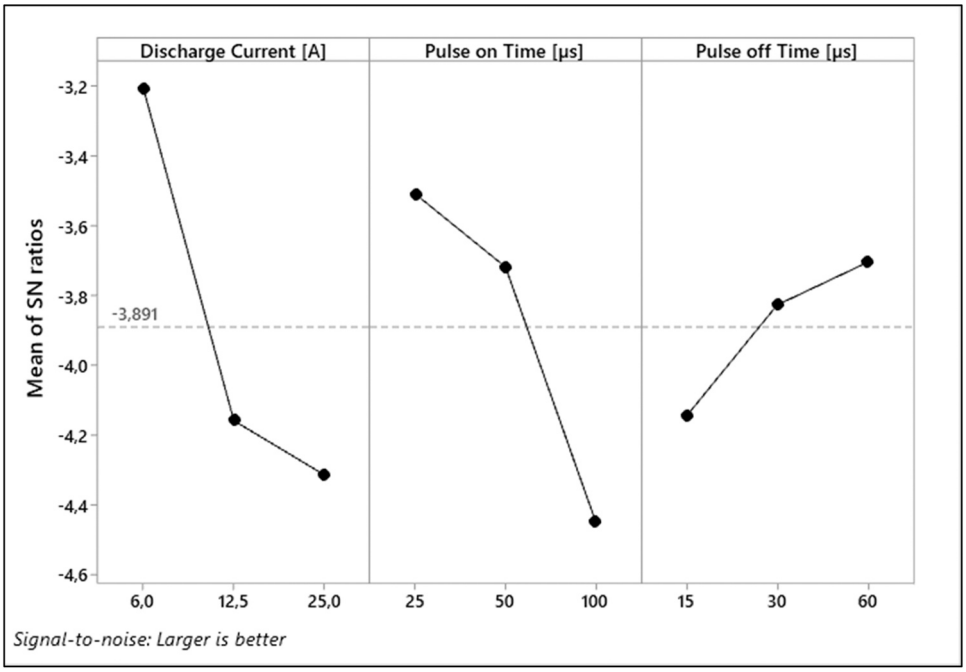

Fig. 10. Effect of machining parameters on GRG.

Table 4
Analysis of variance for GRG.

Parameter	DF	SS	MS	F	P	PCR
Ip	2	0.037448	0.018724	33.79	0.0001	44.23
Ton	2	0.024364	0.012182	21.98	0.0005	28.77
Toff	2	0.004968	0.002484	4.48	0.0494	5.87
Ip*Ton	4	0.008637	0.002159	3.9	0.0482	10.20
Ip*Toff	4	0.001104	0.000276	0.5	0.7384	1.30
Ton*Toff	4	0.003719	0.00093	1.68	0.2470	4.39
Error	8	0.004433	0.000554			5.24
Total	26	0.084673				100.00
R^2 = 94.7%, R^2(adj)= 82.8%						

Analysis of variance (ANOVA) at 95% confidence level was applied to define the effect of EDM parameters on multiple responses. For the grey relational degrees in Table 4, the F value shows the importance and order of the parameters, and the PCR (in %) shows the effect of the parameters on the performance indicators. In addition, it is given that degrees of freedom (DF), the sum of squares (SS), the mean of squares (MS) and P value, which is indicates the importance of parameters [53]. According to the chosen confidence level ($P < 0.05$), it is seen that the single effect of Ip, Ton, Toff and the interaction effect of Ip*Ton have a significant influence on the GRG. According to the ANOVA result, discharge current is the most important parameter (44.23%), followed by pulse time (28.77%) and pulse interval (5.87%). The high coefficient of determination (R^2) value indicates the usability of the applied TGRA methodology.

The amount of improvement in GRG was determined by performing a verification experiment at the optimum parameters (6 A/25µs/60µs) determined as a result of the analysis. The grey relational grade for MRR, TWR and Ra obtained after this experiment was found to be 0.7713. In Table 5, the experimental GRG results at the estimated GRG and optimum parameters are given comparatively. When the table is examined, the GRG obtained from the validation experiment improved by 23.95% with a difference of 0.15 in the confidence interval limits according to the initial parameter. In this case, grey relational analysis applied with Taguchi methodology for EDM technology yielded applicable results for MRR, TWR and Ra.

Based on the experimental and statistical results, it is possible to make the following inferences. In the mold and tool industry, where advanced ceramics are used, high dimensional accuracy and cost are at the forefront. The high tooling cost and negativities such as crack formation and chipping at the edges of the parts that occur in the processing of these materials with conventional methods have increased the demand for unconventional machining techniques [4,8]. In this context, the use of EDM in the processing of WC-Co, especially in complex geometries, can reduce the cost while keeping the desired surface and geometric integrity in the part at the right level. However, it should be noted that tool wear and excessive cutting affect the dimensional accuracy (in terms of width, length and depth) of the workpiece. The presented study showed that machining parameters underlie changes in tool wear and keyway surface quality. By examining the effect of post-EDM machining parameters on dimensional accuracy, the quality performance of the keyway can be improved. For this purpose, higher machining speed and lower tool wear can be achieved by applying multiple optimization results, as well as improving the surface quality and performance of the keyway.

Table 5
Comparison of predicted and experimental results.

	Initial parameters	Optimum Parameter	
		Predicted	Experimental
Levels	*Ip2Ton2Toff2*	*Ip1Ton1Toff3*	*Ip1Ton1Toff3*
MRR (g/min)	0.0165		0.004185
TWR (g/min)	0.00307		0.000619
Ra (µm)	4.069		2.2942
GRG	0.622	0.7546	0.7713
Improvement in GRG = 0.15 or 23.95%			

Conclusions

In this study, a keyway was opened on WC-Co material by die-sinking EDM method. Discharge current, pulse time and pulse interval were used as variable parameters in the experiments. As a result of the experiments performed according to the Taguchi L27 index, the effects of variable parameters on the measured performance indicators (MRR, TWR and Ra) results were analyzed. The results obtained are summarized in the following items.

1. According to the experimental and statistical analysis, it was determined that as the discharge current increases, all of the performance indicators increase. With the increase of the pulse time, Ra increased at a certain rate, while TWR decreased. When the pulse interval was increased, it was observed that MRR, TWR and Ra decreased.
2. The 3D topographic images taken to better define the surface morphology of the machining parameters showed that the amount of peaks and craters on the machined surface decreased and their size expanded with the increase of Ip. As the Ton increased, the thermal energy dissipated in the unit area decreased due to the expanding discharge diameter, resulting in craters with the larger width but the lower depth. On the other hand, increasing the Toff resulted in better debris removal and improved surface roughness. On the other hand, increasing the Toff resulted in better debris removal and improved surface roughness.
3. Micro-valley, craters, debris, globules and a low-thickness white layer were found in the images taken from the processed surface. In addition, it has been observed that micro cracks and craters that may affect the strength of the machined part do not penetrate into the core of the WC material.
4. ANOVA results showed that Ip, Ton and Toff affected GRG values by 44.23%, 28.77% and 5.87%, respectively. Therefore, the discharge current was the most important parameter for simultaneously optimizing the performance indicators. In addition, statistical analysis indicated that the dual effect of Ip*Ton (10.20%) was significant.
5. As a result of TGRA, optimum parameters were determined as discharge current of 6 A, pulse time of 25 µs and pulse interval of 60 µs. When the results of the validation experiment and the initial parameters were compared, it was observed that the GRG improved by 23.95%.
6. These results will not only help achieve the dimensional accuracy and surface quality required for mounting situations in such materials but will also contribute to sustainability. In addition, research can be carried out in environmentally friendly dielectric liquid media in order to contribute more to sustainability.

Declaration of Competing Interest

The authors declare that they have no known competing financial interests or personal relationships that could have appeared to influence the work reported in this paper.

References

[1] Ayode Otitoju, T., Ugochukwu Okoye, P., Chen, G., Li, Y., Onyeka Okoye, M., Li, S., 2020, Advanced ceramic components: Materials, fabrication, and applications. Journal of Industrial and Engineering Chemistry, 85:34–65. https://doi.org/10.1016/j.jiec.2020.02.002.

[2] Salamon, D., 2014, Advanced Ceramics. Advanced Ceramics for Dentistry. first ed. Elsevier, Massachusetts: 103–122.
[3] Carter, C.B., Norton, M.G., 2013, Ceramic Materials: Science and Engineering. second ed. Springer-Verlag, New York. https://doi.org/10.1007/978-1-4614-3523-5.
[4] Rakshit, R., Das, A.K., 2019, A review on cutting of industrial ceramic materials. Precision Engineering, 59:90–109. https://doi.org/10.1016/j.precisioneng.2019.05.009.
[5] Basha, S.M., Basha, M.M., Raj, G.V.P., Venkaiah, N., Sankar, M.R., 2020, Past and current trends in electric discharge based machining of silicon carbide. Materials Today: Proceedings, 26:542–548. https://doi.org/10.1016/j.matpr.2019.12.135.
[6] Diaz, O.G., Garcia Luna, G., Liao, Z., Axinte, D., 2019, The new challenges of machining ceramic matrix composites (CMCs): review of surface integrity. International Journal of Machine Tools and Manufacture, 139:24–36. https://doi.org/10.1016/j.ijmachtools.2019.01.003.
[7] Kruusing, A., Leppävuori, S., Uusimäki, A., Petrêtis, B., Makarova, O., 1999, Micromachining of magnetic materials. Sensors and Actuators A: Physical, 74:45–51. https://doi.org/10.1016/S0924-4247(98)00343-4.
[8] Bilal, A., Jahan, M.P., Talamona, D., Perveen, A., 2019, Electro-discharge machining of ceramics: a review. Micromachines, 10:10. https://doi.org/10.3390/mi10010010.
[9] Liang, Y., Dutta, S.P., 2001, Application trend in advanced ceramic technologies. Technovation, 21:61–65.
[10] Groover, M.P., 2010, Fundamentals of Modern Manufacturing. fourth ed. John Wiley & Sons, New Jersey.
[11] Palanikumar, K., Davim, J.P., 2013, 5 - Electrical discharge machining: study on machining characteristics of WC/Co composites. Davim JP, (Ed.). Machining and Machine-Tools Woodhead Publishing: 135–168. https://doi.org/10.1533/9780857092199.135.
[12] Bhadauria, G., Jha, S.K., Roy, B.N., Dhakry, N.S., 2018, Electrical-discharge machining of tungsten carbide (WC) and its composites (WC-Co) – a review. Materials Today: Proceedings, 5:24760–24769. https://doi.org/10.1016/j.matpr.2018.10.274.
[13] Puertas, I., Luis, C.J., 2012, Optimization of EDM conditions in the manufacturing process of B4C and WC-Co conductive ceramics. International Journal of Advanced Manufacturing Technology, 59:575–582. https://doi.org/10.1007/s00170-011-3509-x.
[14] Pachaury, Y., Tandon, P., 2017, An overview of electric discharge machining of ceramics and ceramic based composites. Journal of Manufacturing Processes, 25:369–390. https://doi.org/10.1016/j.jmapro.2016.12.010.
[15] Shirguppikar, S.S., Patil, M.S., Ghorapade, V., 2020, Grey fuzzy multiobjective optimization of process parameters for dry electro discharge machining process. Materials Today: Proceedings, 27:671–676. https://doi.org/10.1016/j.matpr.2020.02.234.
[16] Lin, Y.-C., Chen, Y.-F., Lin, C.-T., Tzeng, H.-J., 2008, Electrical discharge machining (EDM) characteristics associated with electrical discharge energy on machining of cemented tungsten carbide. Materials and Manufacturing Processes, 23:391–399. https://doi.org/10.1080/10426910801938577.
[17] Lee, S.H., Li, X., 2003, Study of the surface integrity of the machined workpiece in the EDM of tungsten carbide. Journal of Materials Processing Technology, 139:315–321. https://doi.org/10.1016/S0924-0136(03)00547-8.
[18] Çakıroğlu, R., Günay, M., 2020, Comprehensive analysis of material removal rate, tool wear and surface roughness in electrical discharge turning of L2 tool steel. Journal of Materials Research and Technology, 9:7305–7317. https://doi.org/10.1016/j.jmrt.2020.04.060.
[19] Agarwal, N., Shrivastava, N., Pradhan, M.K., 2020, Optimisation of edm process parameters using jaya algorithm. Materials Today: Proceedings, 24:825–834. https://doi.org/10.1016/j.matpr.2020.04.391.
[20] Amorim, F.L., Weingaertner, W.L., Bassani, I.A., 2010, Aspects on the optimization of die-sinking EDM of tungsten carbide-cobalt. Journal of the Brazilian Society of Mechanical Sciences and Engineering, 32:496–502. https://doi.org/10.1590/S1678-58782010000500009.
[21] Singh, J., Sharma, R.K., 2018, Multi-objective optimization of green powder-mixed electrical discharge machining of tungsten carbide alloy. in: Proceedings of the Institution of Mechanical Engineers, Part C: Journal of Mechanical Engineering Science, 232:2774–2786. https://doi.org/10.1177/0954406217727306.
[22] Sarıkaya, M., Yılmaz, V., 2018, Optimization and predictive modeling using S/N, RSM, RA and ANNs for micro-electrical discharge drilling of AISI 304 stainless steel. Neural Computing & Applications, 30:1503–1517. https://doi.org/10.1007/s00521-016-2775-9.
[23] Kumar, P.M., Sivakumar, K., Jayakumar, N., 2018, Multiobjective optimization and analysis of copper–titanium diboride electrode in EDM of monel 400™ alloy. Materials and Manufacturing Processes, 33:1429–1437. https://doi.org/10.1080/10426914.2017.1415439.
[24] Lin, C.L., Lin, J.L., Ko, T.C., 2002, Optimisation of the EDM process based on the orthogonal array with Fuzzy Logic and Grey Relational Analysis method. International Journal of Advanced Manufacturing Technology, 19:271–277. https://doi.org/10.1007/s001700200034.
[25] Yücel, E., Günay, M., 2013, Modelling and optimization of the cutting conditions in hard turning of high-alloy white cast iron (Ni-Hard). in: Proceedings of the Institution of Mechanical Engineers, Part C: Journal of Mechanical Engineering Science, 227:2280–2290. https://doi.org/10.1177/0954406212471755.
[26] Mia, M., 2018, Mathematical modeling and optimization of MQL assisted end milling characteristics based on RSM and Taguchi method. Measurement, 121:249–260. https://doi.org/10.1016/j.measurement.2018.02.017.
[27] Jang, D., Jung, J., Seok, J., 2016, Modeling and parameter optimization for cutting energy reduction in MQL milling process. International Journal of Precision Engineering and Manufacturing-Green Technology, 3:5–12. https://doi.org/10.1007/s40684-016-0001-y.
[28] Prakash, C., Singh, S., Singh, M., Verma, K., Chaudhary, B., Singh, S., 2018, Multi-objective particle swarm optimization of EDM parameters to deposit HA-coating on biodegradable Mg-alloy. Vacuum, 158:180–190. https://doi.org/10.1016/j.vacuum.2018.09.050.
[29] J, Kanchana, V, Prasath, Vijayan, Krishnaraj, Priyadharshini B, Geetha, 2019, Multi response optimization of process parameters using grey relational analysis for milling of hardened Custom 465 steel. Procedia Manufacturing, 30:451–458. https://doi.org/10.1016/j.promfg.2019.02.064.
[30] Rapeti, P., Pasam, V.K., Rao Gurram, K.M., Revuru, R.S., 2018, Performance evaluation of vegetable oil based nano cutting fluids in machining using grey relational analysis-a step towards sustainable manufacturing. Journal of Cleaner Production, 172:2862–2875. https://doi.org/10.1016/j.jclepro.2017.11.127.
[31] Günay, M., Meral, T., 2020, Modelling and multiresponse optimization for minimizing burr height, thrust force and surface roughness in drilling of ferritic stainless steel. Sādhanā, 45:273. https://doi.org/10.1007/s12046-020-01490-3.
[32] Kacal, A., Yıldırım, F., 2013, Application of grey relational analysis in high-speed machining of hardened AISI D6 steel. in: Proceedings of the Institution of Mechanical Engineers, Part C: Journal of Mechanical Engineering Science, 227:1566–1576. https://doi.org/10.1177/0954406212466792.
[33] Yaşar, N., Günay, M., Kılık, E., Ünal, H., 2020, Multiresponse optimization of drillability factors and mechanical properties of chitosan-reinforced polypropylene composite. 0892705720939163 Journal of Thermoplastic Composite Materials.https://doi.org/10.1177/0892705720939163.
[34] Kuo, Y., Yang, T., Huang, G.-W., 2008, The use of grey relational analysis in solving multiple attribute decision-making problems. Computers & Industrial Engineering, 55:80–93. https://doi.org/10.1016/j.cie.2007.12.002.
[35] Nguyen, P.H., Banh, T.L., Mashood, K.A., Tran, D.Q., Dong Pham, V., Muthuramalingam, T., et al., 2020, Application of TGRA-based optimisation for machinability of high-chromium tool steel in the EDM process. Arabian Journal for, 45:5555–5562. https://doi.org/10.1007/s13369-020-04456-z.
[36] Günay, M., 2022, Modeling and multiple optimization in face milling of hardfacing welding applied steel: force, roughness, power. 09544062211065998 in: Proceedings of the Institution of Mechanical Engineers, Part C: Journal of Mechanical Engineering Science.https://doi.org/10.1177/09544062211065998.
[37] Tamura, T., Kobayashi, Y., 2004, Measurement of impulsive forces and crater formation in impulse discharge. Journal of Materials Processing Technology, 149:212–216. https://doi.org/10.1016/j.jmatprotec.2003.10.063.
[38] Singh, H., Shukla, D.K., 2012, Optimizing electric discharge machining parameters for tungsten-carbide utilizing thermo-mathematical modelling. International Journal of Thermal Sciences, 59:161–175. https://doi.org/10.1016/j.ijthermalsci.2012.03.017.
[39] Guu, Y.H., Tsai, K.-L., Chen, L.-K., 2007, An experimental study on electrical discharge machining of manganese–zinc ferrite magnetic material. Materials and Manufacturing Processes, 22:66–70. https://doi.org/10.1080/10426910601015949.
[40] Hasçalık, A., Çaydaş, U., 2007, Electrical discharge machining of titanium alloy (Ti–6Al–4V). Applied Surface Science, 253:9007–9016. https://doi.org/10.1016/j.apsusc.2007.05.031.
[41] Jadam, T., Datta, S., 2020, Machinability of Ti-5Al-2.5Sn for electro-discharge machining: an experimental investigation. Sādhanā, 45:238. https://doi.org/10.1007/s12046-020-01479-y.
[42] Kunieda, M., Kobayashi, T., 2004, Clarifying mechanism of determining tool electrode wear ratio in EDM using spectroscopic measurement of vapor density. Journal of Materials Processing Technology, 149:284–288. https://doi.org/10.1016/j.jmatprotec.2004.02.022.
[43] Koyano, T., Suzuki, S., Hosokawa, A., Furumoto, T., 2016, Study on the effect of external hydrostatic pressure on electrical discharge machining. Procedia CIRP, 42:46–50. https://doi.org/10.1016/j.procir.2016.02.184.
[44] Guu, Y.H., Hou, M.T.-K., 2007, Effect of machining parameters on surface textures in EDM of Fe-Mn-Al alloy. Materials Science and Engineering: A, 466:61–67. https://doi.org/10.1016/j.msea.2007.02.035.
[45] Kumar, S., Singh, R., Singh, T.P., Sethi, B.L., 2009, Surface modification by electrical discharge machining: a review. Journal of Materials Processing Technology, 209:3675–3687. https://doi.org/10.1016/j.jmatprotec.2008.09.032.
[46] Ming, W., Xie, Z., Cao, C., Liu, M., Zhang, F., Yang, Y., et al., 2022, Research on EDM performance of renewable dielectrics under different electrodes for machining SKD11. Crystals, 12:291. https://doi.org/10.3390/cryst12020291.
[47] Liu, S., Thangaraj, M., Moiduddin, K., Al-Ahmari, A.M., 2022, Influence of adaptive gap control mechanism and tool electrodes on machining titanium (Ti-6Al-4V) alloy in EDM process. Materials, 15:513. https://doi.org/10.3390/ma15020513.
[48] Schulze, H.-P., Herms, R., Juhr, H., Schaetzing, W., Wollenberg, G., 2004, Comparison of measured and simulated crater morphology for EDM. Journal of Materials Processing Technology, 149:316–322. https://doi.org/10.1016/j.jmatprotec.2004.02.016.
[49] Shabgard, M., Ahmadi, R., Seyedzavvar, M., Oliaei, S.N.B., 2013, Mathematical and numerical modeling of the effect of input-parameters on the flushing efficiency of plasma channel in EDM process. International Journal of Machine Tools and Manufacture, 65:79–87. https://doi.org/10.1016/j.ijmachtools.2012.10.004.
[50] Cusanelli, G., Hessler-Wyser, A., Bobard, F., Demellayer, R., Perez, R., Flükiger, R., 2004, Microstructure at submicron scale of the white layer produced by EDM technique. Journal of Materials Processing Technology, 149:289–295. https://doi.org/10.1016/j.jmatprotec.2003.11.047.
[51] Guu, Y.H., Hocheng, H., Chou, C.Y., Deng, C.S., 2003, Effect of electrical discharge machining on surface characteristics and machining damage of AISI D2 tool steel. Materials Science and Engineering: A, 358:37–43. https://doi.org/10.1016/S0921-5093(03)00272-7.
[52] Qu, J., Riester, L., Shih, A.J., Scattergood, R.O., Lara-Curzio, E., Watkins, T.R., 2003, Nanoindentation characterization of surface layers of electrical discharge machined WC–Co. Materials Science and Engineering: A, 344:125–131. https://doi.org/10.1016/S0921-5093(02)00395-7.
[53] Uzun, H., Meral, T., Günay, M., 2020, Modelling and optimization of burr height in fiber laser drilling of ferritic stainless steel. İmalat Teknolojileri ve Uygulamaları, 1:32–39.